Appl. Phys. Lett. 102, 251901 (2013); doi: 10.1063/1.4811825
Published by the AIP Publishing LLC.
Journal Homepage: http://apl.aip.org/

Effects of Sequential Tungsten and Helium Ion Implantation on Nano-indentation Hardness of Tungsten

D.E.J. Armstrong, P.D Edmondson, S.G. Roberts

Department of Materials, University of Oxford, Parks Road, Oxford, OX1 3PH UK.

Abstract

To simulate neutron and helium damage in a fusion reactor first wall sequential self-ion implantation up to 13dpa followed by helium-ion implantation up to 3000appm was performed to produce damaged layers of ~2μm depth in pure tungsten. The hardness of these layers was measured using nanoindentation and studied using transmission electron micrcroscopy. Substantial hardness increases were seen in helium implanted regions, with smaller hardness increases in regions which had already been self-ion implanted, thus containing pre-existing dislocation loops. This suggests that, for the same helium content, helium trapped in distributed vacancies gives stronger hardening than helium trapped in vacancies condensed into dislocation loops.

Keywords: Tungsten; ion implantation; helium; radiation damage; nuclear materials

Tungsten is the most important candidate material for plasma facing surfaces in any future nuclear fusion power device [1], due to its combination of low sputtering rate, low activation under transmutation, and good thermal conductivity [2]. In a plasma-facing role it will be subjected to some of the most extreme conditions of any engineering materials; surface temperatures of over 1000^{o}C, damage levels of up to 50dpa/year from 14.1MeV neutrons, transmutation-induced compositional changes of up to 5at% over operational lifetimes [3] and implantation of helium directly from the plasma [4]. Degradation of tungsten in these conditions will limit the component lifetime and have adverse effects on the fusion plasma efficiency due to ingress of sputtered tungsten atoms and dust. The combination of displacement damage from neutrons and helium (present due to both transmutation and injection from the plasma) will result in significant mechanical changes in the tungsten. Understanding the mechanisms behind these effects will be vital in modelling failure mechanisms of plasma- facing tungsten. Studies of helium in tungsten have concentrated on the mechanisms behind the formation of bubbles [5], voids [6] and “nano-fuzz” [7]; however very little work has been carried out to assess the influence of helium on tunsgten’s mechanical properties.

Nanoindentation has been used to study the effects of helium implantation on the mechanical properties of advanced nuclear steels. Chen et al. performed simultaneous and sequential Fe^+ ion and He^+ ion implantations into a PM2000 ODS steel (in the as-received state and cold-rolled to 30% and 70% reduction in thickness), to 31dpa and 18appm/dpa of helium. They saw a hardness increase due to the implantation of 1.15GPa in the as-received material, 0.23GPa in the 30% rolled and 0.2GPa for the 70% rolled. For the two rolled materials, hardness increases were within 1 standard deviation of the unirradiated hardness. This suggests that the rolling produces defects which act as sinks for helium and displacement damage and which reduce their hardening effect. Kogler et al. [8] also carried out Fe/He implantations on PM2000, in as-received and heat-treated conditions, performing both sequential and simultaneous implantations to 52dpa and 20.7appm He/dpa. In the as-received materials the simultaneous implantation gave significantly higher hardening (1GPa) than the sequential implantation, whereas in the heat-treated case the material implantated simultaneously with Fe and He was only 0.3GPa harder than that implanted sequentially. Hunn et al [9] performed helium implantation on 316LN stainless steel using 360keV helium ions to a level of 332appm. This was seen to give large increases of hardness of up to 2GPa in the region of maximum damage, which was associated with the formation of helium bubbles, whereas Fe^+ ion implantation at similar dpa damage levels gave rise to increases in hardness 50% lower. These studies have shown that helium implantation can have a stronger hardening effect than self-ion implantation as well as differences in hardness between sequential and simultaneous implantations in feritic alloys. However while there have been several studies on the mechanical properties of both neutron [10, 11] and self-ion implanted tungsten alloys[12, 13], where dramatic increases in hardness, of up to 3GPa, have been observed, there has been no work on the effect of helium implantation on the mechanical properties of tungsten. This paper reports the changes in hardness in pure tungsten after self ion implantation with tungsten ions, implantation with helium ions and sequential implantation of tungsten followed by helium.

High purity (99.99%) polycrystalline tungsten, (as used in a previous study on brittle to ductile transition behaviour [14]) from Metals Crystals and Oxides (UK) was sectioned into 1mm thick slices and mechanically polished using diamond suspensions followed by chemomechanical polishing with colloidal silica to produce a high quality surface. Ion implantation was carried out at the Surrey National Ion Beam Centre, UK, using a 2MV Tandem accelerator. Tungsten ion implantation was carried out at 300°C using 2MeV W^+ ions. One of two doses was used, either $3.5x10^{13}$ ions/cm^2 or $1.05x10^{15}$ions/cm^2. SRIM (stopping range of ions in matter) software was used

to convert doses to a displacement per atom values (dpa) using a displacement energy of 68eV [15]. This gives 0.4dpa for the low dose and 13dpa for the higher dose at peak damage. Samples were mounted so that half of the sample was blanked from the ion beam. Following the tungsten ion implantation, one of two helium ion implantations was performed on the same samples. These were carried out at 300°C using He+ at 0.05 MeV, 0.1 MeV, 0.2 MeV, 0.3 MeV, 0.4 MeV,0.6 MeV,0.8 MeV,1.0 MeV,1.2 MeV,1.4 MeV,1.6 MeV, and 1.8MeV. The He+ implantations produced damage levels of either 0.02 dpa or 0.25 dpa and a helium concentration of ≈300appm or 3000appm; see figure 1. For the helium implantation, half the previously unimplanted region and half the previously W^+ ion implanted region was now exposed to the He+ beam and the other half blanked. The resulted in each sample having four distinct regions, as shown in figure 1, with each having experienced the same thermal cycle. Implantation doses will be referred to as 0W,LDW,HDW and 0He,LDHe,HDHe. Each sample comprised four regions with the various combinations of W and He; for example the region 0W-LDHe was implanted with He+ to 300appm only whereas the region HDW-HDHe was implanted with W+ to 13dpa and then He+ to 3000appm. Three samples were prepared: (1) LDW + LDHe; (2) HDW + LDHe; (3) HDW + HDHe.

Nanoindentation was performed on all four areas of each sample using an MTS Nanoindenter XP (MTS, TN, USA) and the "continuous stiffness measurement" (CSM) method allowing hardness and stiffness to be measured continuously at all indentation depths. Arrays of 16 indents to 200nm depth and 4 indents to 2000nm depth were placed in each section of the three samples. Figure 2 shows four typical load-displacement curves over first 2mN load for each of four regions of the HDW-LDHe (13dpa W^+ / 300appm He+) sample (for clarity, in each case only four are shown of the 16 indentation tests made). In the unimplanted region (figure 2a) an initial Hertzian response can be observed at low loads followed by several distinct large pop in events; beyond the pop-in there is considerable variation between the load-displacement curves for the individual indents. In figure 2b (HDW) the tungsten ion implantation suppresses the occurrence of the initial pop-in events, with only a small number of very small pop-ins occurring, although the variation in the load-displacement curves between individual indents is similar to that seen in unimplanted material. The effect of low-dose helium ion implantation is shown in figure 2c; again the initial pop-ins have been almost totally suppressed as compared to the unimplanted material. The material is significantly harder than either W-implanted or unimplanted material. In addition the spread in the data is suppressed with all curves (four are shown) lying almost exactly on top of each other. Figure 2d (HDW - LDHe) is similar to 0W-LDHe in that initial-pop ins are suppressed, hardness is increased and the spread in data drops compared to unimplanted or HDW implanted tungsten..

Figure 3a shows hardness as a function of indenter displacement into the surface for conditions 0W-0He, LDW-0He, 0W-HDHe, and LDW-HDHe. The LDW implanted sample shows a maximum increase in hardness over the unimplanted material of 0.8GPa at 170nm indenter displacement but shows no increase in hardness by 600nm indenter displacement. The HDHe implanted material shows a significant increase in hardness to 11.2GPa at 130nm displacement, and is still significantly harder (7.0GPa) than the unimplanted material at 900nm displacement. The LDW-HDHe implanted material shows a slightly smaller increase in hardness over the first 300nm than the HDHe sample, reaching a peak hardness of 10.6GPa at 200nm displacement. Both the HDHe and LDW-HDHe implanted materials show the same hardness –depth profile for displacement greater than 300nm, roughly the depth of penetration of the W ions (figure 1c).

Figure 3b shows the average hardness of 16 indents over an indenter displacement range of 0-200nm (the range at which there would be expected to be influence from both W+ and He+ implantations) for all 8 different implantation conditions. This data are summarised in figure 3c which shows the average hardness between 100nm and 200nm for each condition. The unimplanted material has a hardness of 6.0GPa. Under W+ ion implantation alone the hardness of the HDW sample increases significantly more than the LDW sample (average hardness of 8GPa as compared to 6.5GPa). The HDHe condition (11 GPa) hardens more than the LDHe condition (7.2GPa). The increase in hardness for the HDHe condition which has a damage level of 0.25dpa and 3000appm He+ is significantly higher than that seen for the LDW condition which has a similar damage level (0.4dpa).

For the highest helium dose , pre-implantation with W appears to reduce the overall hardening effect: hardness decreases in the sequence HDHe, LDW-HDHe, HDW-LDHe. In the HDW-LDHe condition the measured hardness is slightly greater than that for the LDW, and identical to that for the HDW condition.

To study the damage incurred during helium implantation, transmission electron microscopy (TEM) was performed using a JEOL3000F TEM. Figure 4 shows transmission electron microscopy images (TEM) from a HDW-HDHe sample. Three different grains were studied, but no visible bubbles of helium were found. It is not possible to infer from TEM the location of helium in tungsten when it is not in resolvable bubbles, but He may be present in smaller He-vacancy clusters below the resolution limit of the TEM. It is known that helium is highly mobile in tungsten even at room temperature [16]. Work by Debelle et al. [17] using positron annihilation spectroscopy and nuclear reaction analysis showed no release of the helium when helium-implanted tungsten was annealed at 1100°C in vacuum, indicating that the helium is strongly bound to the vacancies. This is in agreement with modelling by Lee et al. [18] who show, using density functional theory (DFT), that

helium will migrate to vacancies rather than remain in interstitial or substitutional sites. The helium ion implantation will create vacancies during the collision events, which would be expected to become rapidly associated with helium forming stable structures. This has been confirmed in work by Lhuillier [19] who showed that helium implanted above the threshold energy for vacancy formation is fully retained when the damage level is above 0.1dpa, while when helium was implanted at an energy below the vacancy formation energy, the helium was fully released on annealing at 1600°C. It is known that helium vacancy clusters form in tungsten, as observed in work by Lhuillier. et al. [20] using positron annihilation spectroscopy.

The difference in hardness between areas which were implanted first with tungsten ions followed by helium ions and those only implanted with helium ions is significant. The tungsten implanted regions will have a very high initial defect density. Work on similar materials implanted to damage levels from 0.4dpa to 33dpa, with W+ ions at 2MeV [13], showed prismatic dislocation loop densities of $5.7x10^{22}m^{3}$ to $1.61x10^{23}m^{3.}$ Loops were either of b=a/2<100> (~40%) or b=a/2<111> (~60%) type, from 1-8nm in diameter, and of both vacancy and interstitial types, in roughly equal numbers.

We suggest that the hardening due to these combined implantations results from two defect types: dislocation loops and helium-vacancy complexes. Both appear to have strong hardening effects. However, the results presented here suggest that for a given helium fraction, the strongest hardening is produced if the helium atoms are present as helium-vacancy complexes; these are invisible to the TEM techniques used here. Molecular dynamics modelling by Yang et al. [21] for bcc iron shown a strong interaction between edge dislocations and large vacancy-helium clusters, which increase with the number of helium atoms per vacancy. This may be the mechanism for the large increase in hardness in tungsten seen after the helium implantation.

For samples implanted with tungsten before helium implantation, some of the He+ ions are likely to be trapped at the dislocation loops reducing the trapping in vacancies. In Figure 3a, the hardness of the HDW-HDHe sample is seen to be lower than the 0W-HDHe material, but only at indenter penetration of less than 300nm, the depth range over which a hardening effect of the W+ implantation is found. At greater depths than this the hardness-depth profile for HDW-HDHe follows the same curve as for the 0W-HDHe sample. The HDW-HDHe material shows a lower hardness than the LDW-HDHe, implying the higher tungsten implantation dose has introduced a higher density of dislocation loops for the helium to trap at in this sample, further reducing the He trapped in vacancies. In the LDHe sample, the hardness of the sample to HDW-LDHE region is higher than the hardness of the 0W-LDHe region. The HDW-LDHe region shows the same hardness as the 0W-HDW

region. Here, the hardening from the dislocation loops formed by the W+ implantation appears to dominate over the hardness increase due to helium in solution.

Further work on the exact nature of the damage caused by the sequential implantations and the precise location of the helium is needed to understand more completely the mechanisms which underlie these hardness changes, as are studies on how the helium affects both the fracture toughness and brittle to ductile transition temperature in tungsten if it is to be used in high helium environments. To study the helium location small angle X-ray scattering experiments could be performed to look for He-bubbles of a size below the resolution of TEM which may also have a significant effect on hardness[22], due to their interactions with mobile dislocations. Position annihilation spectroscopy [19] and thermal desorption spectroscopy [23] would also allow study of location of the helium in greater detail –complementing the TEM already performed. For further evaluation of the effects of helium on mechanical properties other than hardness such as yield stress and fracture behaviour advanced micromechanical testing using focused ion beam machined pillars [24, 25] and microcantilers [26-28] are being employed. However undoubtedly these dramatic hardness increases resulting from helium implantation into tungsten represent a particular concern for the application of tungsten, which is already inherently brittle, in fusion reactor environments.

Acknowledgments

DEJA thanks Culham Centre for Fusion Energy for funding via a Research Fellowship at St Edmund Hall, Oxford. All authors acknowledge support from EPSRC grants EP/H018921/1, EP/G004676/1, and EP/F004451/1, and the support of staff at the National Ion Beam Centre, University of Surrey, UK.

[1] Rieth M, Dudarev SL, Gonzalez de Vicente SM, Aktaa J, Ahlgren T, Antusch S, Armstrong DEJ, Balden M, Baluc N, Barthe MF, Basuki WW, Battabyal M, Becquart CS, Blagoeva D, Boldyryeva H, Brinkmann J, Celino M, Ciupinski L, Correia JB, De Backer A, Domain C, Gaganidze E, García-Rosales C, Gibson J, Gilbert MR, Giusepponi S, Gludovatz B, Greuner H, Heinola K, Höschen T, Hoffmann A, Holstein N, Koch F, Krauss W, Li H, Lindig S, Linke J, Linsmeier C, López-Ruiz P, Maier H, Matejicek J, Mishra TP, Muhammed M, Muñoz A, Muzyk M, Nordlund K, Nguyen-Manh D, Opschoor J, Ordás N, Palacios T, Pintsuk G, Pippan R, Reiser J, Riesch J, Roberts SG, Romaner L, Rosiński M, Sanchez M, Schulmeyer W, Traxler H, Ureña A, van der Laan JG, Veleva L, Wahlberg S, Walter M, Weber T, Weitkamp T, Wurster S, Yar MA, You JH, Zivelonghi A. Journal of Nuclear Materials (2013) 432 482.
[2] Rieth M. Journal of Nuclear Materials (2011) 417 463.
[3] Gilbert MR, Sublet JC. Nuclear Fusion (2011) 51 043005.
[4] Raj B, Vijayalakshmi M, Rao PRV, Rao KBS. Mrs Bulletin (2008) 33 327.
[5] Iwakiri H, Yasunaga K, Morishita K, Yoshida N. Journal of Nuclear Materials (2000) 283 1134.

[6] Hashimoto N, Hunn JD, Parikh N, Gilliam S, Gidcumb S, Patnaik B, Snead LL. Journal of Nuclear Materials (2005) 347 307.
[7] Baldwin MJ, Doerner RP. Journal of Nuclear Materials (2010) 404 165.
[8] Kogler R, Anwand W, Richter A, Butterling M, Ou X, Wagner A, Chen CL. Journal of Nuclear Materials (2012) 427 133.
[9] Hunn JD, Lee EH, Byun TS, Mansur LK. Journal of Nuclear Materials (2000) 282 131.
[10] He JC, Tang GY, Hasegawa A, Abe K. Nuclear Fusion (2006) 46 877.
[11] Tanno T, Hasegawa A, He JC, Fujiwara M, Nogami S, Satou M, Shishido T, Abe K. Materials Transactions (2007) 48 2399.
[12] Armstrong DEJ, Wilkinson AJ, Roberts SG. Physica Scripta (2011) T145 014076.
[13] Armstrong DEJ, Yi X, Marquis EA, Roberts SG. Journal of Nuclear Materials (2013) 432 428.
[14] Giannattasio A, Yao Z, Tarleton E, Roberts SG. Philosophical Magazine (2010) 90 3947.
[15] International A. ASTM E521 - 96(2009) Standard Practice for Neutron Radiation Damage Simulation by Charged-Particle Irradiation. ASTM International, West Conshohocken, PA, 2009.
[16] Kornelsen EV. Canadian Journal of Physics (1970) 48 2812.
[17] Debelle A, Barthe MF, Sauvage T, Belamhawal R, Chelgoum A, Desgardin P, Labrim H. Journal of Nuclear Materials (2007) 362 181.
[18] Lee S-C, Choi J-H, Lee JG. Journal of Nuclear Materials (2009) 383 244.
[19] Lhuillier PE, Belhabib T, Desgardin P, Courtois B, Sauvage T, Barthe MF, Thomann AL, Brault P, Tessier Y. Journal of Nuclear Materials (2011) 416 13.
[20] Lhuillier PE, Debelle A, Belhabib T, Thomann AL, Desgardin P, Sauvage T, Barthe MF, Brault P, Tessier Y. Journal of Nuclear Materials (2011) 417 504.
[21] Yang L, Zu XT, Gao F, Peng SM, Heinisch HL, Long XG, Kurtz RJ. Physica B-Condensed Matter (2010) 405 1754.
[22] Suresh K, Ohnuma M, Oba Y, Kishimoto N, Das P, Chini TK. Journal of Applied Physics (2010) 107.
[23] Kornelsen EV, Vangorkum AA. Journal of Nuclear Materials (1980) 92 79.
[24] Grieveson EM, Armstrong, D.E.J, Xu, S. Roberts, S.G. Journal Nuclear Materials (2012) 430 119.
[25] Kiener D, Hosemann P, Maloy SA, Minor AM. Nature Materials (2011) 10 608.
[26] Armstrong DEJ, Wilkinson AJ, Roberts SG. Philosophical Magazine Letters (2011) 91 394.
[27] Armstrong DEJ, Wilkinson AJ, Roberts SG. Probing Mechanics at Nanoscale Dimensions (2009) 1185 7.
[28] Wurster S, Motz C, Jenko M, Pippan R. Advanced Engineering Materials (2010) 12 61.

Figure Captions

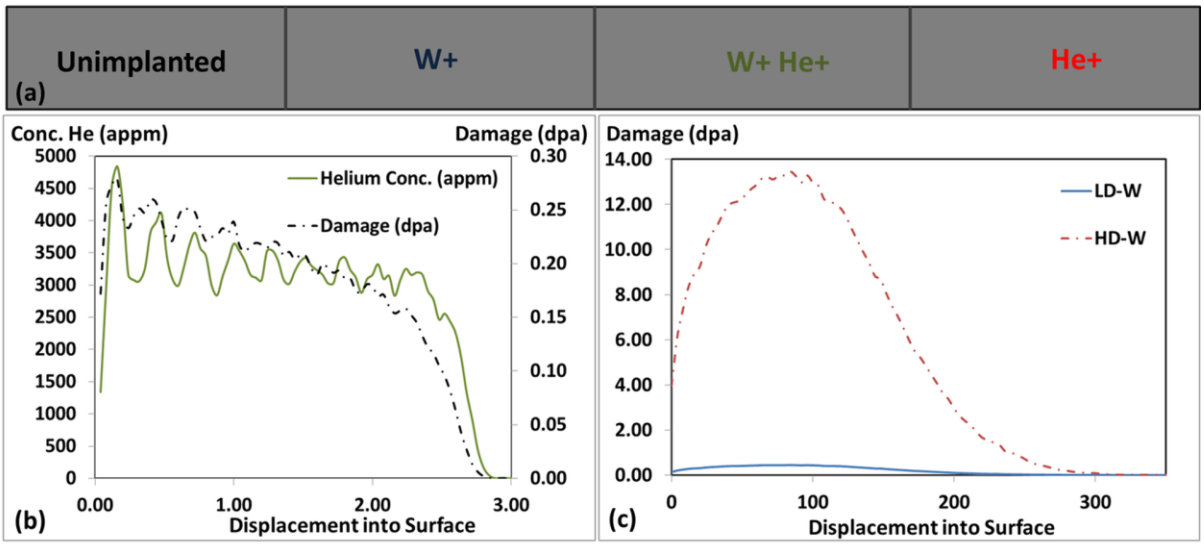

Figure 1: a) Schematic of sample after W^+ and He^+ implantation showing 4 regions produced. b) Predicted damage and helium concentration profiles from multiple-energy HD He+ implantation. c) Predicted damage profile from W+ implantation.

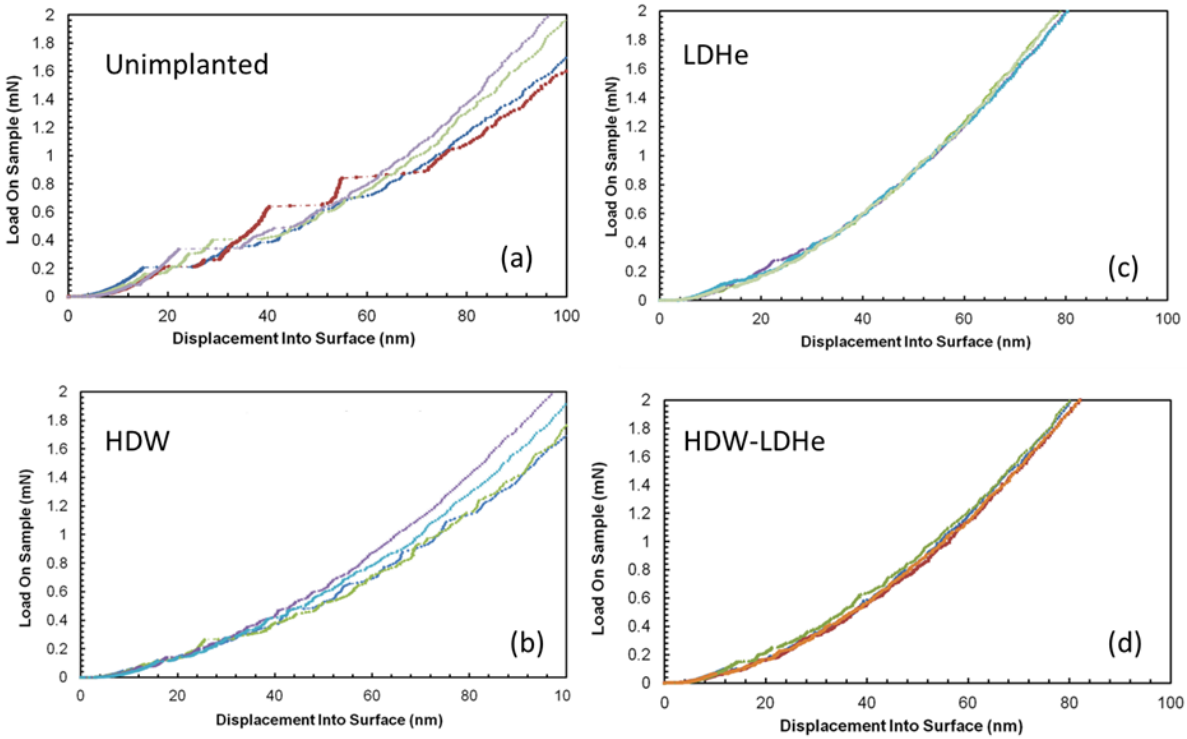

Figure 2: Typical nanoindentation load-displacement curves for a) 0W-0He, b) HDW-0He, c) 0W-LDHe, d) HDW-LDHe

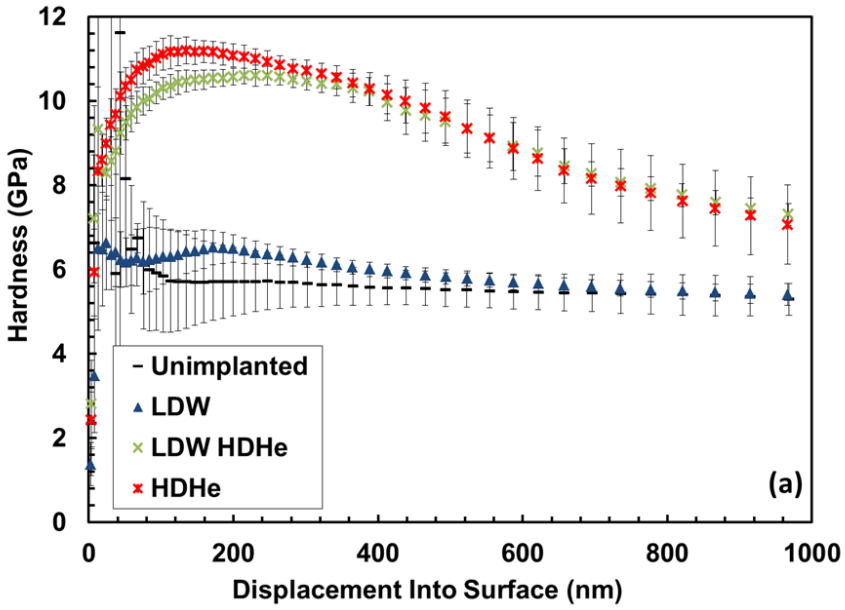
Hardness (GPa)
Displacement Into Surface (nm)
Unimplanted
LDW
LDW HDHe
HDHe
(a)

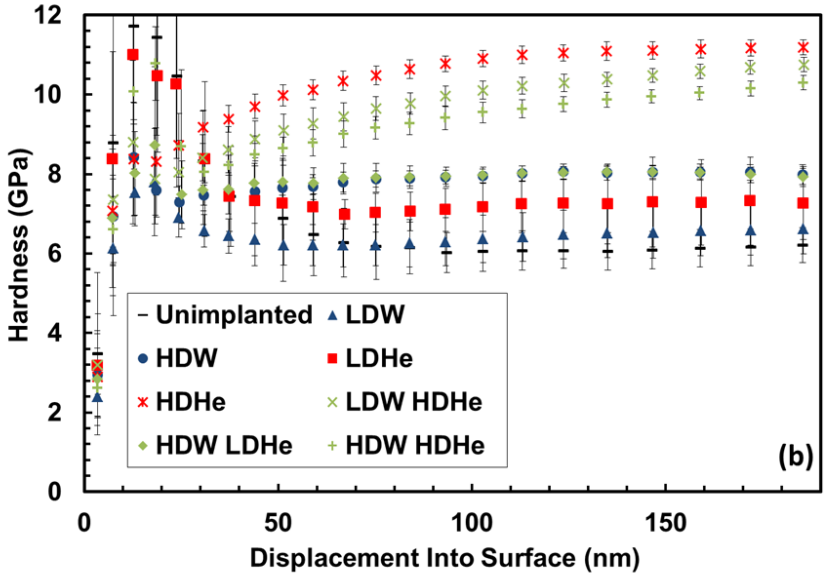
Hardness (GPa)
Displacement Into Surface (nm)
Unimplanted
LDW
HDW
LDHe
HDHe
LDW HDHe
HDW LDHe
HDW HDHe
(b)

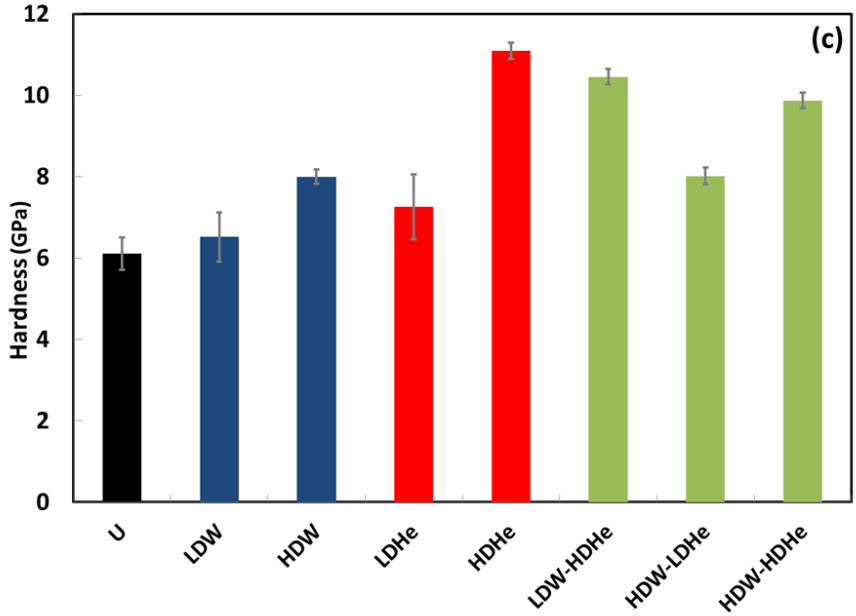
Hardness (GPa)
(c)
U
LDW
HDW
LDHe
HDHe
LDW-HDHe
HDW-LDHe
HDW-HDHe

Figure3: a) Hardness-displacement curves for 0W0He, LDW-0He, 0W-HDHe, LDW-HDHe, showing tungsten ion damage effect extends for ≈300nm and the helium damage range extends for over 1000nm. b) hardness-displacement curves for all implantation conditions from 0-200nm. c) Summary of average hardness values of all 8 conditions between 100 and 200nm.

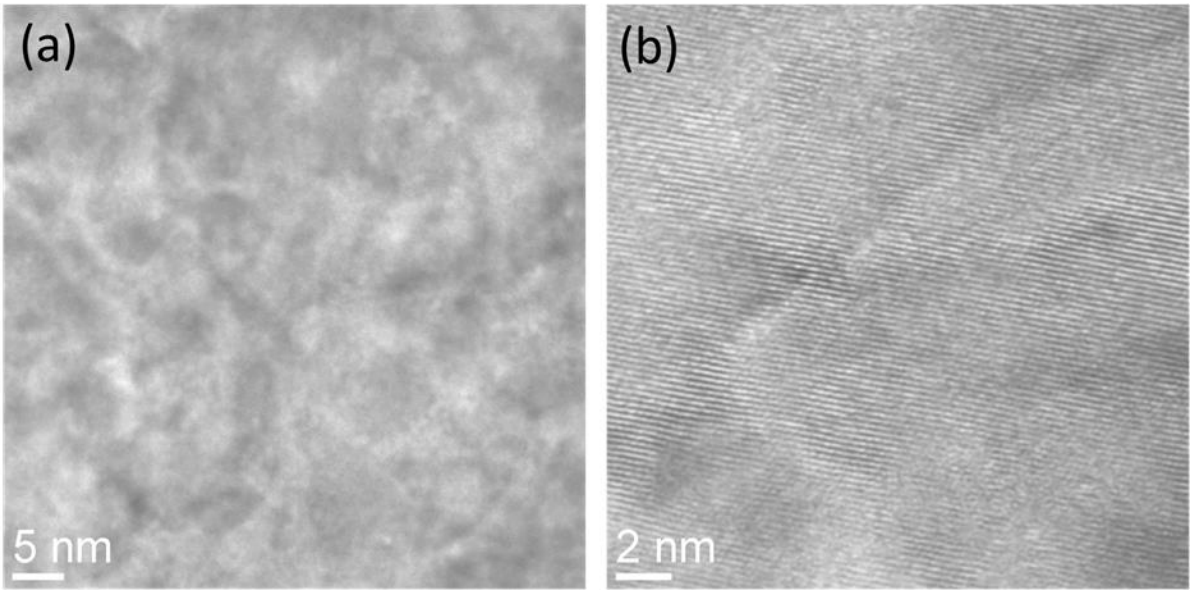

Figure4: TEM micrograph of the 3000appm He implanted pure W. The image was recorded at ~1µm underfocus. No Fresnel contrast was observed in a through-focus series indicating no He bubbles are present.